Detection of Bell correlations at finite temperature from matter-wave interference fringes

A. Niezgoda,[1] J. Chwedeńczuk,[1] L. Pezzé,[2] and A. Smerzi[2]
[1]*Faculty of Physics, University of Warsaw, Ulica Pasteura 5, PL-02-093 Warszawa, Poland*
[2]*QSTAR, INO-CNR and LENS, Largo Enrico Fermi 2, 50125 Firenze, Italy*

(Received 8 March 2019; published 24 June 2019)

We show that matter-wave interference fringes formed by two overlapping atomic clouds can yield information about the nonlocal Bell correlations. To this end, we consider a simple atomic interferometer, where the clouds are released from the double-well potential and the relative phase is estimated from the density fit to this interference pattern. The Bell correlations can be deduced from the sensitivity of the phase obtained in this way. We examine the relation between these two quantities for a wide range of ground states of the double-well, scanning through the attractive and the repulsive interactions. The presented analysis includes the effects of finite temperature, when excited states are thermally occupied. We also consider the impact of the spatial resolution of the single-atom detectors, the fluctuations of the energy mismatch between the wells, and the atom-number fluctuations. These results establish a link between the fundamental (nonlocality) and the application-oriented (quantum metrology) aspects of entanglement.

DOI: 10.1103/PhysRevA.99.062115

I. INTRODUCTION

The interference pattern obtained after time-of-flight imaging [1] is a direct probe of phase coherence in ultracold gases [2,3]. Interference effects have been used to probe the superfluid to Mott-insulator quantum phase transition in an optical lattice [4], detect the Berezinskii-Kosterlitz-Thouless transition in two-dimensional quantum gases [5], demonstrate collapse and revivals of phase coherence [6], reveal the quantum statistics of bosonic [7] and fermionic [8] atoms via Hanbury-Brown and Twiss correlations, measure the effective spin length of a condensate in a double-well system [9,10], and study the evolution of the relative phase in Josephson experiments [11–13]. Moreover, interference of condensates released from an optical lattice has been used to demonstrate mode entanglement [14] and is a tool to extract the Renyi entropy in optical lattices [15]. Multipartite entanglement between atoms in a double-well potential [16–19] can be detected by the phase uncertainty obtained in repeated interference experiments with Bose-Einstein condensates [20].

In this manuscript, we show that interference fringes formed by two weakly linked Bose-Einstein condensates—initially trapped in a double-well potential and overlapping after free expansion—can reveal Bell correlations between atoms through the sole analysis of the one-body density distribution. We relate the quantum phase sensitivity obtained from the analysis of the density pattern after the matter-wave expansion to the criteria for witnessing Bell correlations based on the first- and second-order correlation functions of bosons derived in Ref. [21] (see also Refs. [22–26] for recent studies). Bell's correlations—recently observed in atomic ensembles [27–30]—are a strong form of entanglement necessary to violate Bell's inequalities [31,32] and eventually demonstrate the nonlocality of quantum mechanics [33–35]. Differently from existing experimental studies [27–29], where Bell correlations between neutral atoms have been observed using internal degrees of freedom (atomic hyperfine states) and the measurement of the composite spin vector required a number of manipulations of the system, in our case Bell correlations are witnessed using external degrees of freedom and by the observation of the interference pattern. To run a complete Bell test in such a configuration, qubits should be spatially separated to ensure that the local transformations are independent. This could be achieved for instance by immersing the quantum gas in a superlattice, consisting of an array of double-well potentials [36]. We demonstrate that Bell correlations in the Bose gas are naturally present in the ground state of the system without requiring, in the case of attractive interaction, further manipulation. Our study takes into account relevant experimental imperfections such as finite temperature, finite spatial resolution of single-atom detectors, and the fluctuations of the energy mismatch between the two wells of the trapping potential as well as of the total number of atoms.

II. MODEL AND METHODS

We consider an ultracold Bose gas trapped in a double-well potential and with tunable interparticle interaction [13,37,38]. For a sufficiently high tunneling barrier and relatively weak interaction, the system can be described in a two-mode approximation (see Ref. [38] for a review). In this case, the bosonic field operator is $\hat{\Psi}(\mathbf{r},t)=\psi_a(\mathbf{r},t)\hat{a}+\psi_b(\mathbf{r},t)\hat{b}$, where $\hat{a}$ and $\hat{b}$ annihilate a particle in the left or right well of the potential, respectively, and $\psi_{a,b}(\mathbf{r},t)$ are the corresponding (real) spatial wave functions centered around the minima of the double-well trap satisfying $\int d\mathbf{r}\,\psi^2_{a,b}(\mathbf{r},t)=1$ and $\int d\mathbf{r}\,\psi_a(\mathbf{r},t)\psi_b(\mathbf{r},t)=0$. The normalization condition sets $\int d\mathbf{r}\langle\hat{\Psi}^\dagger(\mathbf{r},t)\hat{\Psi}(\mathbf{r},t)\rangle=\langle\hat{a}^\dagger\hat{a}+\hat{b}^\dagger\hat{b}\rangle=N$, where N is the conserved total number of particles. Within this two-mode approximation, the system can be described by the bosonic

Josephson junction Hamiltonian

$$\hat{H} = -\hat{J}_x + \frac{\Lambda}{N}\hat{J}_z^2 + \delta\hat{J}_z, \tag{1}$$

where

$$\hat{J}_x = \frac{\hat{a}^\dagger\hat{b} + \hat{b}^\dagger\hat{a}}{2}, \quad \hat{J}_y = \frac{\hat{a}^\dagger\hat{b} - \hat{b}^\dagger\hat{a}}{2i}, \quad \hat{J}_z = \frac{\hat{a}^\dagger\hat{a} - \hat{b}^\dagger\hat{b}}{2} \tag{2}$$

is the triad of the angular momentum operators. In Eq. (1) the parameters are rescaled to the Josephson tunneling energy E_J. And so, $\Lambda = U/E_J$ rules the competition between interaction and tunneling—it can be positive or negative, depending on whether the interaction strength is repulsive or attractive, respectively. The parameter δ depends on the energy mismatch between the two wells. It should be noticed that, for $\delta = 0$, the ground state of Eq. (1) undergoes a second-order quantum phase transition at $\Lambda = -1$ between a paramagnetic (at $\Lambda > -1$) and a ferromagnetic ($\Lambda < -1$) phase [38–42]. For a fixed value of $\Lambda < -1$ and by tuning the energy mismatch δ, we see that the system has a first-order quantum phase transition with a discontinuous jump of the population imbalance. First- and second-order quantum phase transitions in this system have been experimentally observed in Ref. [37].

After the preparation of the condensate in the double-well system (we consider the zero-temperature cases as well as the finite-temperature cases), we give a phase shift φ between the two modes. This is obtained by applying an energy imbalance δ_φ between the two modes for a time t_φ such that $\varphi = \delta_\varphi t_\varphi$ (we set $\hbar \equiv 1$), assuming that the effect of tunneling and interaction is negligible during the phase acquisition time, $E_J t_\varphi, U t_\varphi \ll \varphi$. We also assume that φ is reproducible in repeated independent experiments. After phase acquisition, the trap is switched off and the wave packets, initially localized in the two wells, expand and overlap, giving the field operator

$$\hat{\Psi}(\mathbf{r}, t_f) = \phi(\mathbf{r}, t_f)\left(\hat{a}e^{\frac{i}{2}(\mathbf{kr}+\varphi)} + \hat{b}e^{-\frac{i}{2}(\mathbf{kr}+\varphi)}\right), \tag{3}$$

where $\phi(\mathbf{r}, t_f)$ is the common envelope, $\mathbf{k} = 2\mathbf{r}_0 m/t_f$, $2\mathbf{r}_0$ is the vector pointing from the center of one well to the other, t_f is the time of flight, and m is the mass of a single atom. This gives the normalized one-body density:

$$\varrho(\mathbf{r}, t_f; \varphi) = \frac{\langle\hat{\Psi}^\dagger(\mathbf{r}, t_f)\hat{\Psi}(\mathbf{r}, t_f)\rangle}{N} = \frac{1}{N}|\phi(\mathbf{r}, t_f)|^2 \times \langle\hat{a}^\dagger\hat{a} + \hat{b}^\dagger\hat{b} + \hat{a}^\dagger\hat{b}e^{-i(\mathbf{kr}+\varphi)} + \hat{b}^\dagger\hat{a}e^{i(\mathbf{kr}+\varphi)}\rangle. \tag{4}$$

Using the definitions from Eq. (2) we obtain

$$\varrho(\mathbf{r}, t_f; \varphi) = |\phi(\mathbf{r}, t_f)|^2 \times \left[1 + \frac{2}{N}(\langle\hat{J}_x\rangle\cos(\mathbf{kr}+\varphi) + \langle\hat{J}_y\rangle\sin(\mathbf{kr}+\varphi))\right]. \tag{5}$$

We take $\langle\hat{J}_y\rangle = 0$ throughout the text—this is satisfied for all the ground states of the double-well potential, as well as for all eigenstates of the Hamiltonian (1), which have real coefficients of the expansion into the occupation basis (i.e., the basis of eigenstates of the $\hat{J}_z$ operator). This condition is altered neither by the thermal fluctuations nor by other sources of noise considered below. In such a case, the visibility of the fringes is

$$\nu = \frac{\varrho_{\max} - \varrho_{\min}}{\varrho_{\max} + \varrho_{\min}} = \frac{2}{N}|\langle\hat{J}_x\rangle|, \text{ where} \tag{6a}$$

$$\varrho_{\max/\min} = |\phi(\mathbf{r}, t_f)|^2(N \pm 2|\langle\hat{J}_x\rangle|). \tag{6b}$$

This gives

$$\varrho(\mathbf{r}, t_f; \varphi) = \frac{\langle\hat{\Psi}^\dagger(\mathbf{r}, t_f)\hat{\Psi}(\mathbf{r}, t_f)\rangle}{N} = 1 + \nu\cos(\mathbf{k}\cdot\mathbf{r} + \varphi). \tag{7}$$

Note that we typically neglect the envelope $|\phi(\mathbf{r}, t_f)|^2$ in the experiment; when the central interference fringes are inspected, the envelope can be safely taken as constant.

The phase φ can be estimated by measuring the position of atoms and then fitting the one-body density $\varrho(\mathbf{r}, t_f; \varphi_{\text{est}})$, Eq. (7), using the least-squares method, with φ_{est} as a free parameter. This gives an estimator φ_{est} of φ which is unbiased [20]; $\overline{\varphi_{\text{est}}} = \varphi$ as the number of experiments tends to infinity, where the overline denotes statistical averaging. The variance of this estimator, taken as a measure of the sensitivity of the double-well interferometer, is equal to [20]

$$\Delta^2\varphi_{\text{est}} = \frac{1}{N}\left[\xi_\phi^2 + \frac{\sqrt{1-\nu^2}}{\nu^2}\right], \tag{8}$$

where $\xi_\phi^2 = N\langle\hat{J}_y^2\rangle/\langle\hat{J}_x\rangle^2$ is the spin-squeezing parameter [38]. The condition $\xi_\phi^2 < 1$ implies squeezing of the $\hat{J}_y$ spin component, which is generally indicated as phase-squeezing [43,44]. We introduce the parameter

$$\mathcal{A} \equiv N\Delta^2\varphi_{\text{est}} - 1 = \xi_\phi^2 + \frac{\sqrt{1-\nu^2} - \nu^2}{\nu^2}. \tag{9}$$

Sub-shot-noise sensitivity, i.e., $\Delta^2\varphi_{\text{est}} < \frac{1}{N}$, in the estimation of φ is equivalent to $\mathcal{A} < 0$.

In this manuscript we relate Eq. (8) to the witness of Bell's correlations introduced in Refs. [21,27], namely $B(\theta) \equiv \langle\hat{B}(\theta)\rangle$, where the operator

$$\hat{B}(\theta) = 2N\cos^2\left(\frac{\theta}{2}\right) - 4\hat{J}_1 + 8\sin^2\left(\frac{\theta}{2}\right)\left[-\hat{J}_1\sin\left(\frac{\theta}{2}\right) + \hat{J}_2\cos\left(\frac{\theta}{2}\right)\right]^2 \tag{10}$$

contains only one- and two-body operators. Here the subscripts "1" and "2" denote a pair of orthogonal directions. The system contains Bell correlations if $B(\theta) < 0$.

To relate $\Delta^2\varphi_{\text{est}}$—or equivalently the parameter $\mathcal{A}$—to the witness of Bell correlations, it is convenient to apply the transformations $\hat{J}_1 = \hat{J}_x\cos(\frac{\theta}{2}) - \hat{J}_y\sin(\frac{\theta}{2})$ and $\hat{J}_2 = \hat{J}_x\sin(\frac{\theta}{2}) + \hat{J}_y\cos(\frac{\theta}{2})$ to Eq. (10), giving [27]

$$B(\theta) = 2N\cos^2\left(\frac{\theta}{2}\right) - 4\langle\hat{J}_x\rangle\cos\left(\frac{\theta}{2}\right) + 8\sin^2\left(\frac{\theta}{2}\right)\langle\hat{J}_y^2\rangle. \tag{11}$$

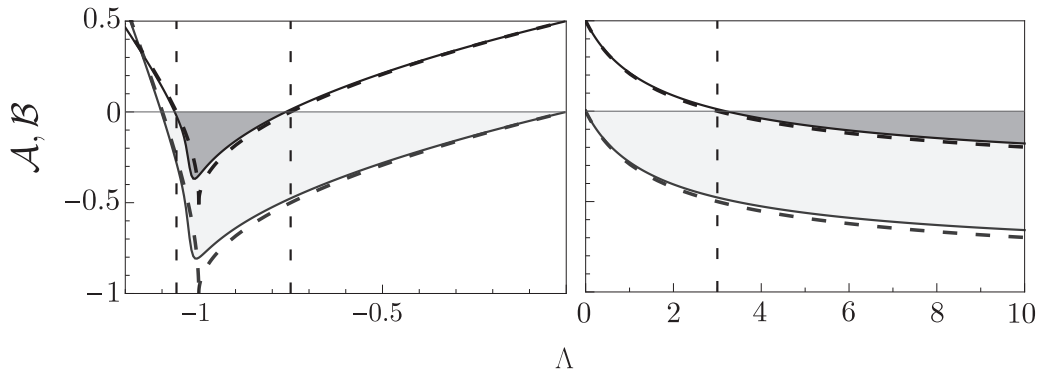

FIG. 1. The numerical (solid lines) and analytical (dashed lines) results for coefficients $\mathcal{A}$ (gray lines) and $\mathcal{B}$ (black lines) as a function of the interaction strength Λ for both attractive (left panel) and repulsive (right panel) interactions ($T = 0$, $\delta = 0$, and $N = 1000$). The shaded areas indicate the regimes $\mathcal{A} \leqslant 0$ (lighter area) and $\mathcal{B} \leqslant 0$ (darker area). Vertical lines for $\Lambda = \frac{-3}{2\sqrt{2}}, -\frac{3}{4}$, and 3 indicate the analytical solution for $\mathcal{B} = 0$.

This equation can be minimized analytically with respect to θ and the minimum is reached for

$$\cos\left(\frac{\theta_0}{2}\right) = \frac{\nu}{2\left(1-\xi_\phi^2\nu^2\right)}. \tag{12}$$

Replacing Eq. (12) into Eq. (11) we obtain that Bell's correlations are witnessed when

$$\mathcal{B} \equiv \xi_\phi^2 + \frac{\sqrt{1-\nu^2}-1}{2\nu^2} < 0, \tag{13}$$

the result first obtained in Ref. [27]. Finally, the parameter $\mathcal{A}$ from Eq. (9) and $\mathcal{B}$ from (13) are related by a simple function of the fringe visibility:

$$\mathcal{B} = \mathcal{A} + f(\nu), \tag{14}$$

where $f(\nu) = 1 - \frac{\sqrt{1-\nu^2}+1}{2\nu^2}$ and $\mathcal{A}$ is given by Eq. (9). Thus the fit of the one-body function to the interference pattern brings not only the knowledge about the phase and its sensitivity [20] but also the knowledge about the Bell correlations in the system.

III. NOISELESS CASE

First we take the noiseless case—the system is prepared in the ground state of Eq. (1) with $\delta = 0$—and provide the analytical expressions for $\mathcal{A}$ and $\mathcal{B}$ in the semiclassical approximation [45,46], valid for $N \gg 1$. In the regime of attractive interactions, the system remains phase-squeezed for $-(1+\sqrt{5})/2 < \Lambda < 0$ [47]. In the semiclassical approach this range must be split into $-1 \lesssim \Lambda < 0$, when the visibility is almost constant ($\nu \approx 1$), and $-(1+\sqrt{5})/2 < \Lambda \lesssim -1$, when the visibility quickly drops. In the former case, we have $\xi_\phi^2 \approx \sqrt{1+\Lambda}$ and

$$\mathcal{A} \approx \sqrt{1+\Lambda} - 1, \quad \mathcal{B} \approx \sqrt{1+\Lambda} - 1/2. \tag{15}$$

The condition $\mathcal{B} < 0$ reduces to $\xi_\phi^2 < 1/2$, which is achieved for $\Lambda < -3/4$. In the latter case, when $-(1+\sqrt{5})/2 < \Lambda \lesssim -1$, we have $\xi_\phi^2 \approx |\Lambda|\sqrt{\Lambda^2-1}$ and $\nu \approx 1/|\Lambda|$, giving

$$\mathcal{A} \approx 2|\Lambda|\sqrt{\Lambda^2-1} - 1, \quad \mathcal{B} \approx \frac{3}{2}|\Lambda|\sqrt{\Lambda^2-1} - \frac{\Lambda^2}{2}. \tag{16}$$

The condition $\mathcal{B} < 0$ gives $\Lambda > -3/(2\sqrt{2})$. The analytical expressions (15) and (16) are quite accurate for sufficiently large N, except around $\Lambda = -1$ where the approximations used to derive these expressions break down [47].

Finally, the repulsive interactions ($0 \leqslant \Lambda \ll N^2$) must be considered separately. This is because the ground state of Eq. (1) is number-squeezed in this regime, namely $\xi_N^2 = N(\Delta\hat{J}_z)^2/\langle\hat{J}_x\rangle^2 < 1$ [9,10,38]. A further rotation through $\pi/2$ around the x axis is necessary to transform the number-squeezing into the phase-squeezing. This rotation is achieved, for instance, by a quench of the tunneling for a time $t_{\pi/2}E_J = \pi/2$ such that $t_{\pi/2}U \ll 1$ is negligible. This transformation preserves $\nu \approx 1$ and yields

$$\mathcal{A} \approx \frac{1}{\sqrt{1+\Lambda}} - 1, \quad \mathcal{B} \approx \frac{1}{\sqrt{1+\Lambda}} - \frac{1}{2}. \tag{17}$$

The condition to observe Bell correlations, $\mathcal{B} < 0$, is $\xi_\phi^2 < 1/2$, which is fulfilled for $\Lambda > 3$. In Fig. 1 we plot $\mathcal{A}$ and $\mathcal{B}$ as a function of Λ and for $N = 1000$: analytical results (solid lines) are well reproduced by the numerical calculation (dashed lines, obtained via exact diagonalization). The slight discrepancy between the numerical results and the analytical prediction for $\Lambda > 0$ is due to the finite atom number and the assumption $\nu \approx 1$ used in Eq. (17).

IV. NOISY CASE

In a more realistic scenario, we include the noise coming from four different sources.

A. Energy imbalance fluctuations

First, we take into account nonvanishing energy imbalance between the wells, i.e., $\delta \neq 0$, which is one of the leading sources of noise in current double-well experiments [13,37]. We model the shot-to-shot fluctuations of δ with a Gaussian distribution of width σ_δ, such that the quantum state of the system is given by a density matrix,

$$\hat{\varrho}_{\sigma_\delta,\Lambda} = \mathcal{N}\int d\delta\, e^{-\frac{\delta^2}{2\sigma_\delta^2}} |\Psi_{\delta,\Lambda}\rangle\langle\Psi_{\delta,\Lambda}|, \tag{18}$$

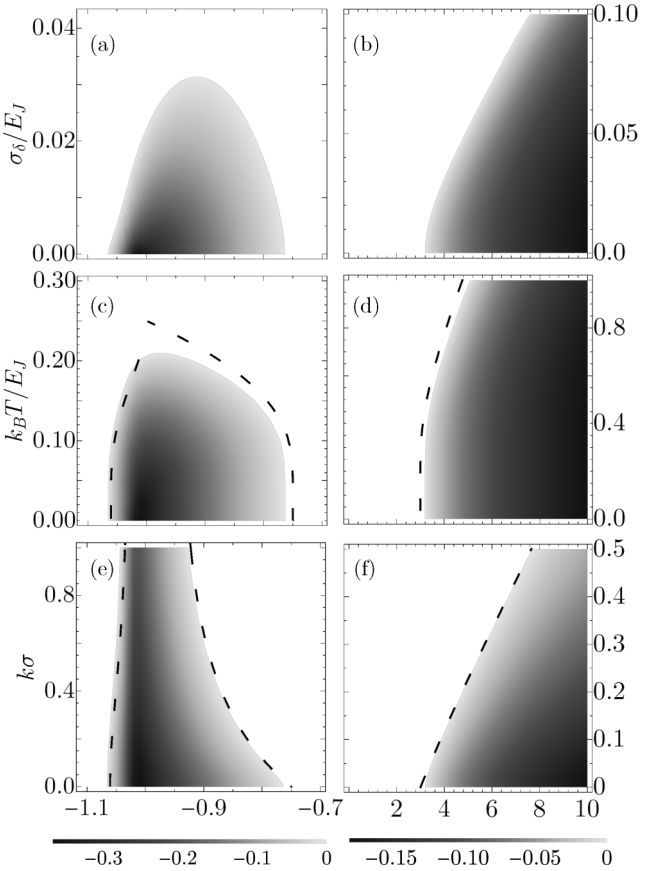

FIG. 2. Parameter regions where the condition $\mathcal{B} < 0$ (shaded area) is fulfilled. Panels (a) and (b) show the effect of energy imbalance (modeled as a normal distribution with width σ_δ) at $T = 0$. Panels (c) and (d) show the finite temperatures T case, for $\sigma_\delta = 0$. Panels (e) and (f) show the effect of the finite resolution σ of spatial detection of the atoms, at $T = 0$ and $\sigma_\delta = 0$. The dashed lines in panels (c)–(f) are analytic predictions for $\mathcal{B} = 0$ obtained from Eq. (22). In all panels $N = 1000$.

where $\mathcal{N}$ is the normalization constant and $|\Psi_{\delta,\Lambda}\rangle$ is the ground state of Eq. (1) for fixed values of Λ and δ. We calculate $\mathcal{A}$ and $\mathcal{B}$ for Eq. (18) and plot the results in Figs. 2(a) and 2(b). There, we show the regions of $\mathcal{B} < 0$: the darker the shade of gray is, the more negative the value of $\mathcal{B}$ is. With growing σ_δ the range of values of Λ for which the Bell correlations are witnessed by $\mathcal{B}$ shrinks, and the effect is much more pronounced for attractive interactions. The regions of SSN sensitivity, $\mathcal{A} < 0$ shrinks proportionally, according to Eq. (14).

B. Thermal fluctuations

Next, we consider the effects of nonzero temperature. First, we construct the density matrix at thermal equilibrium for the Hamiltonian (1), namely

$$\hat{\varrho}_{\rm th} = \frac{1}{\mathcal{Z}} \sum_{n=0}^{N} |\Psi_n\rangle\langle\Psi_n| e^{-\beta E_n}, \tag{19}$$

where $\mathcal{Z}$ is the partition function, $\hat{H}|\Psi_n\rangle = E_n|\Psi_n\rangle$, and $\beta = E_J/(k_BT)$ (where k_B is the Boltzmann constant). The coefficients $\mathcal{A}$ and $\mathcal{B}$ are obtained from a calculation of the relevant spin moments using $\hat{\varrho}_{\rm th}$, for instance, $\langle \hat{J}_y^2 \rangle_{\rm th} = {\rm Tr}[\hat{\varrho}_{\rm th}\hat{J}_y^2] = \sum_{n=0}^{N} \frac{e^{-\beta E_n}}{\mathcal{Z}} \langle\Psi_n|\hat{J}_y^2|\Psi_n\rangle$. Numerical results are shown in Figs. 2(c) and 2(d). The dashed lines in these panels give $\mathcal{B} = 0$ and are obtained from an analytical expression for the spin-squeezing parameter [47], valid for sufficiently large N,

$$\xi_\phi^2(T) = \begin{cases} |\Lambda|\sqrt{\Lambda^2-1}\coth\left(\frac{\beta\sqrt{\Lambda^2-1}}{2}\right), & \Lambda < -1, \\ \sqrt{1+\Lambda}\coth\left(\frac{\beta\sqrt{1+\Lambda}}{2}\right), & -1 < \Lambda < 0, \\ \frac{1}{\sqrt{1+\Lambda}}\coth\left(\frac{\beta\sqrt{1+\Lambda}}{2}\right), & \Lambda > 0, \end{cases} \tag{20}$$

and assuming $\nu \approx 1$ the numerical results are reproduced quite accurately.

C. Finite resolution

The third source of noise we consider comes from the finite resolution in the detection of the atoms. To model this effect we convolute the density Eq. (7) with a Gaussian probability of detecting an atom at position $\mathbf{r}$ given its true position $\mathbf{r}'$, namely

$$\begin{aligned} \tilde{\varrho}(\mathbf{r}, t_f; \varphi) &= \frac{1}{(\sqrt{2\pi}\sigma)^3} \int d\mathbf{r}\, e^{-\frac{(\mathbf{r}-\mathbf{r}')^2}{2\sigma^2}} \varrho(\mathbf{r}, t_f; \varphi) \\ &= 1 + \tilde{\nu}\cos(\mathbf{k}\cdot\mathbf{r} + \varphi), \end{aligned} \tag{21}$$

where $\tilde{\nu} = \nu e^{-\frac{1}{2}k^2\sigma^2}$ is a blurred visibility. Using $\tilde{\varrho}$, we calculate the sensitivity $\Delta^2\varphi_{\rm est}$ and, from Eq. (14), we obtain the expression for the Bell witness, i.e.,

$$\mathcal{B}(T, \sigma) = \xi_\phi^2(T) + \frac{\sqrt{1-\tilde{\nu}^2}-1}{2\tilde{\nu}^2}. \tag{22}$$

In Figs. 2(e) and 2(f), we show the region of parameters for which $\mathcal{B}(0, \sigma) \leqslant 0$, while the dashed line is the analytical prediction for $\mathcal{B} = 0$.

In Fig. 3 we display the combined effect of these three sources of noise, both on $\mathcal{A}$ and $\mathcal{B}$. In the top row (a), we show that the growth of σ_δ from 0.01 to 0.05 (i.e., from dashed to dash-dotted lines, with fixed $T = 0.1$ and $\sigma = 0.1$) has significant impact, particularly on $\mathcal{B}$ in the negative-Λ regime. This is also visible in the middle row (b) when the temperature rises from $T = 0.1$ to $T = 0.2$ (with fixed $\sigma = 0.1$ and $\sigma_\delta = 0.01$). On the other hand, when the population imbalance fluctuations are fixed at $\sigma_\delta = 0.01$ and the temperature is at $T = 0.2$, a loss of resolution from 0.05 to 0.2 does not have a pronounced effect in either the repulsive-interactions case or the attractive-interactions case, as can be seen in the bottom row (c). Such observations could be helpful for designing future experiments with entangled quantum gases.

D. Atom-number fluctuations

Finally, we take into account the impact of the shot-to-shot atom-number fluctuations. To this end, we follow the method outlined in the supplementary materials of Ref. [27]. We

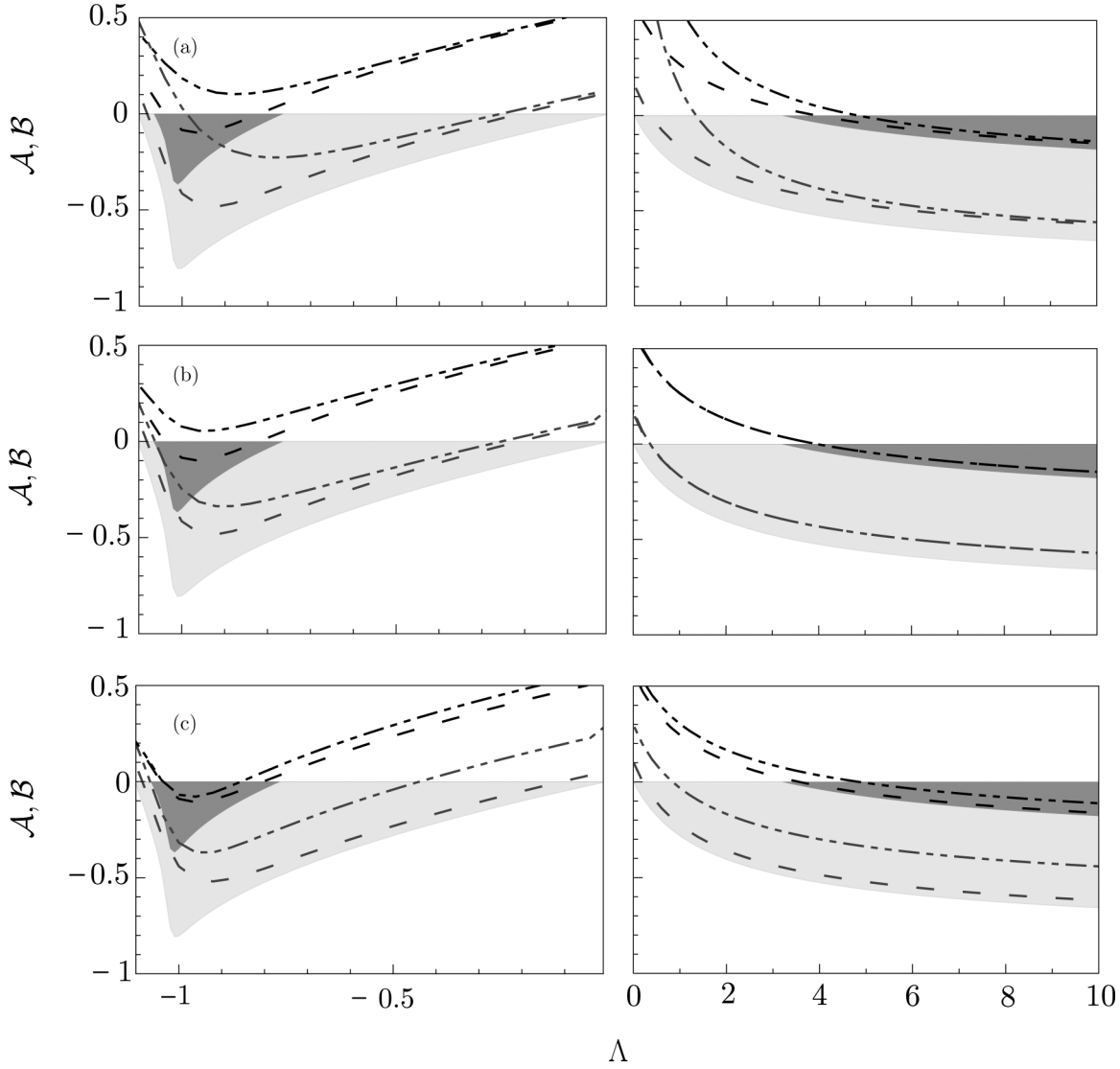

FIG. 3. The accumulated impact of all types of noise on $\mathcal{A}$ (gray lines) and $\mathcal{B}$ (black lines) as a function of the interaction strength Λ for both attractive (left column) and repulsive (right column) interactions. (a) $T = 0.1$, $\sigma = 0.1$, $\sigma_\delta = 0.01$ (dashed lines), and $\sigma_\delta = 0.05$ (dash-dotted lines). (b) $\sigma_\delta = 0.01$, $\sigma = 0.1$, $T = 0.1$ (dashed lines), and $T = 0.2$ (dash-dotted lines). (c) $\sigma_\delta = 0.01$, $T = 0.1$, $\sigma = 0.05$ (dashed lines), and $\sigma = 0.2$ (dash-dotted lines) In all panels $N = 500$. The shaded areas show the regions of Λ where the SSN sensitivity (light gray) and Bell correlations (dark gray) are present in the ideal noise-free case.

construct a mixture,

$$\hat{\varrho}_{\sigma_N,\Lambda} = \sum_{N=0}^{\infty} \mathcal{P}_N |\psi_{N,\Lambda}\rangle\langle\psi_{N,\Lambda}|, \tag{23}$$

where the probability for having N atoms in the system is modeled with a Gaussian function of width σ_N, i.e.,

$$\mathcal{P}_N \propto \exp\left[-\frac{(N-\bar{N})^2}{2\sigma_N^2}\right]. \tag{24}$$

Here $\bar{N}$ is the mean number of atoms in the system and the proportionality stands for the normalization. Also, $|\psi_{N,\Lambda}\rangle$ is the ground-state of the Hamiltonian (1) at $\delta = 0$ with fixed N and Λ.

Since the angular momentum operators act in a fixed-N subspace of the total Hilbert space, the Bell operator from Eq. (10) can be divided by the atom-number operator $\hat{N}$, giving the witness of Bell correlations analogous to Eq. (11), namely

$$b(\theta) = 2\cos^2\left(\frac{\theta}{2}\right) - 4x\cos\left(\frac{\theta}{2}\right) + 8y^2\sin^2\left(\frac{\theta}{2}\right), \tag{25}$$

where we introduced

$$x = \left\langle \frac{\hat{J}_x}{\hat{N}} \right\rangle, \quad y^2 = \left\langle \frac{\hat{J}_y^2}{\hat{N}} \right\rangle, \tag{26}$$

and the average is calculated using the state (23). Next, we optimize this expression with respect to θ and obtain that if

$$\overline{\mathcal{B}} \equiv \frac{y^2}{x^2} + \frac{\sqrt{1-4x^2}-1}{8x^2} < 0 \tag{27}$$

the system is Bell correlated. In Fig. 4 we display $\overline{\mathcal{B}}$ for $\bar{N} = 30$ (top row) with the fluctuations at the shot-noise

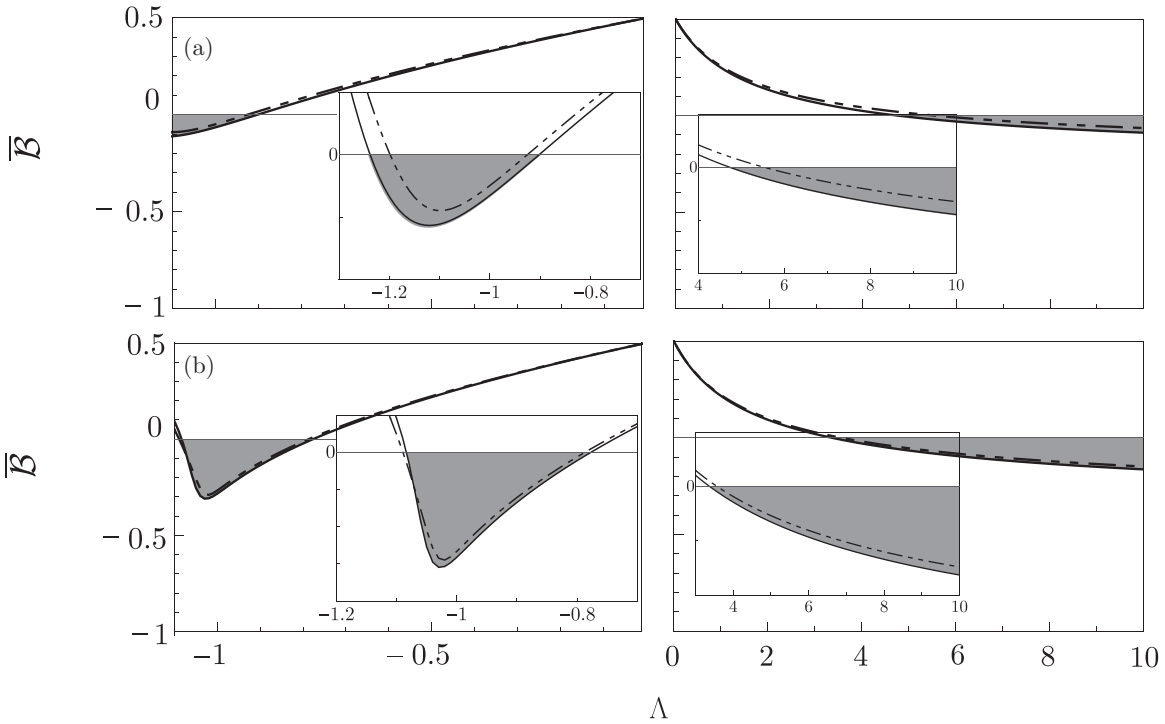

FIG. 4. The Bell witness $\overline{\mathcal{B}}$ in the presence of atom-number fluctuations. (a) $\bar{N} = 30$ with $\sigma_N = \sqrt{\bar{N}}$ (solid line lines) and $\sigma_N = 20$ (dot-dashed lines). (b) $\bar{N} = 300$ and $\sigma_N = \sqrt{\bar{N}}$ (solid lines) and $\sigma_N = 200$ (dot-dashed lines). Gray areas show regions of Λ where the Bell correlations are witnessed by $\mathcal{B}$, i.e., in the absence of atom-number fluctuations.

level, which is typically encountered in the experiments, i.e., $\sigma_N = \sqrt{\bar{N}} \simeq 5.5$ (solid line) and much-exceeding this value ($\sigma_N = 20$, dot-dashed line). The bottom row is for $\bar{N} = 300$ and analogically $\sigma_N = \sqrt{\bar{N}} \simeq 17.3$ (solid line) and $\sigma_N = 200$ (dot-dashed line). These numerical results are contrasted with the ideal case when the atom-number fluctuations are absent (i.e., $\sigma_N \to 0$). When the fluctuations are at the shot-noise level, the difference is hardly noticeable in both the low- and the high-$\bar{N}$ cases. This is because $\mathcal{B}$ is to a good approximation intensive in N [see Eqs. (15), (16), and (17)]. Therefore both x and y^2 weakly depend on N in this regime. Only vast atom-number fluctuations shrink the region of Λ, where the Bell correlations are witnessed by Eq. (25).

V. CONCLUSIONS

We have shown that the observation of the one-body density distribution of atoms released from a double-well potential and forming an interference pattern can witness the existence of nonlocal Bell correlations is this system. This is achieved by a precise link between the precision of phase estimation obtained from a fit of the density to this pattern and the Bell coefficient $\mathcal{B}$ introduced in Refs. [21,27]. We have analyzed the relation between these two quantities for the bosonic Josephson junction Hamiltonian, with both attractive and repulsive interaction, including the effects of finite temperature, energy imbalance between the two wells, finite detection efficiency, and atom-number fluctuations. The two former sources of imperfection have a leading impact on the observation of Bell correlations considered here, while the latter pair is less significant. Our results provide an experimentally feasible method of detecting the Bell correlations and establish a link between the fundamental and the application-oriented aspects of entanglement.

ACKNOWLEDGMENTS

We thank M. Fattori for comments and discussions. A.N. and J.Ch. acknowledge the support of Project No. 2017/25/Z/ST2/03039 funded by the National Science Centre, Poland, under the QuantERA programme. This work is also supported by the QuantERA ERA-NET Cofund in Quantum Technologies projects TAIOL and CEBBEC.

[1] M. Andrews, C. Townsend, H.-J. Miesner, D. Durfee, D. Kurn, and W. Ketterle, Science **275**, 637 (1997).
[2] I. Bloch, J. Dalibard, and W. Zwerger, Rev. Mod. Phys. **80**, 885 (2008).
[3] M. Inguscio and L. Fallani, *Atomic Physics: Precise Measurements and Ultracold Matter* (Oxford University, Oxford, 2013).
[4] M. Greiner, O. Mandel, T. Esslinger, T. W. Hänsch, and I. Bloch, Nature (London) **415**, 39 (2002).

[5] Z. Hadzibabic, P. Krüger, M. Cheneau, B. Battelier, and J. Dalibard, Nature (London) **441**, 1118 (2006).

[6] M. Greiner, O. Mandel, T. W. Hänsch, and I. Bloch, Nature (London) **419**, 51 (2002).

[7] S. Fölling, F. Gerbier, A. Widera, O. Mandel, T. Gericke, and I. Bloch, Nature (London) **434**, 481 (2005).

[8] T. Rom, T. Best, D. Van Oosten, U. Schneider, S. Fölling, B. Paredes, and I. Bloch, Nature (London) **444**, 733 (2006).

[9] J. Esteve, C. Gross, A. Weller, S. Giovanazzi, and M. Oberthaler, Nature (London) **455**, 1216 (2008).

[10] T. Berrada, S. van Frank, R. Bücker, T. Schumm, J.-F. Schaff, and J. Schmiedmayer, Nat. Commun. **4**, 2077 (2013).

[11] F. Cataliotti, S. Burger, C. Fort, P. Maddaloni, F. Minardi, A. Trombettoni, A. Smerzi, and M. Inguscio, Science **293**, 843 (2001).

[12] M. Albiez, R. Gati, J. Fölling, S. Hunsmann, M. Cristiani, and M. K. Oberthaler, Phys. Rev. Lett. **95**, 010402 (2005).

[13] G. Spagnolli, G. Semeghini, L. Masi, G. Ferioli, A. Trenkwalder, S. Coop, M. Landini, L. Pezzè, G. Modugno, M. Inguscio *et al.*, Phys. Rev. Lett. **118**, 230403 (2017).

[14] M. Cramer, A. Bernard, N. Fabbri, L. Fallani, C. Fort, S. Rosi, F. Caruso, M. Inguscio, and M. B. Plenio, Nat. Commun. **4**, 2161 (2013).

[15] R. Islam and R. Ma, Nature (London) **528**, 77 (2015).

[16] L. Pezzé and A. Smerzi, Phys. Rev. Lett. **102**, 100401 (2009).

[17] P. Hyllus, W. Laskowski, R. Krischek, C. Schwemmer, W. Wieczorek, H. Weinfurter, L. Pezzé, and A. Smerzi, Phys. Rev. A **85**, 022321 (2012).

[18] G. Tóth, Phys. Rev. A **85**, 022322 (2012).

[19] L. Pezzé, L. A. Collins, A. Smerzi, G. P. Berman, and A. R. Bishop, Phys. Rev. A **72**, 043612 (2005).

[20] J. Chwedeńczuk, P. Hyllus, F. Piazza, and A. Smerzi, New J. Phys. **14**, 093001 (2012).

[21] J. Tura, R. Augusiak, A. B. Sainz, T. Vértesi, M. Lewenstein, and A. Acín, Science **344**, 1256 (2014).

[22] S. Pelisson, L. Pezzè, and A. Smerzi, Phys. Rev. A **93**, 022115 (2016).

[23] J. Tura, G. De las Cuevas, R. Augusiak, M. Lewenstein, A. Acín, and J. I. Cirac, Phys. Rev. X **7**, 021005 (2017).

[24] M. Fadel and J. Tura, Quantum **2**, 107 (2018).

[25] F. Baccari, J. Tura, M. Fadel, A. Aloy, J.-D. Bancal, N. Sangouard, M. Lewenstein, A. Acín, and R. Augusiak, arXiv:1802.09516.

[26] T. Wasak and J. Chwedeńczuk, Phys. Rev. Lett. **120**, 140406 (2018).

[27] R. Schmied, J.-D. Bancal, B. Allard, M. Fadel, V. Scarani, P. Treutlein, and N. Sangouard, Science **352**, 441 (2016).

[28] S. Wagner, R. Schmied, M. Fadel, P. Treutlein, N. Sangouard, and J.-D. Bancal, Phys. Rev. Lett. **119**, 170403 (2017).

[29] N. J. Engelsen, R. Krishnakumar, O. Hosten, and M. A. Kasevich, Phys. Rev. Lett. **118**, 140401 (2017).

[30] D. K. Shin, S. S. Hodgman, B. M. Henson, T. Wasak, J. Chwedeńczuk, and A. G. Truscott, arXiv:1811.05681.

[31] R. Horodecki, P. Horodecki, M. Horodecki, and K. Horodecki, Rev. Mod. Phys. **81**, 865 (2009).

[32] N. Brunner, D. Cavalcanti, S. Pironio, V. Scarani, and S. Wehner, Rev. Mod. Phys. **86**, 419 (2014).

[33] A. Einstein, B. Podolsky, and N. Rosen, Phys. Rev. **47**, 777 (1935).

[34] J. S. Bell, Physics **1**, 195 (1964).

[35] J. S. Bell, Rev. Mod. Phys. **38**, 447 (1966).

[36] D. Jaksch, C. Bruder, J. I. Cirac, C. W. Gardiner, and P. Zoller, Phys. Rev. Lett. **81**, 3108 (1998).

[37] A. Trenkwalder, G. Spagnolli, G. Semeghini, S. Coop, M. Landini, P. Castilho, L. Pezzè, G. Modugno, M. Inguscio, A. Smerzi *et al.*, Nat. Phys. **12**, 826 (2016).

[38] L. Pezzè, A. Smerzi, M. K. Oberthaler, R. Schmied, and P. Treutlein, Rev. Mod. Phys. **90**, 035005 (2018).

[39] V. Ulyanov and O. Zaslavskii, Phys. Rep. **216**, 179 (1992).

[40] J. Vidal, G. Palacios, and R. Mosseri, Phys. Rev. A **69**, 022107 (2004).

[41] P. Ziń, J. Chwedeńczuk, B. Oleś, K. Sacha, and M. Trippenbach, Europhys. Lett. **83**, 64007 (2008).

[42] P. Buonsante, R. Burioni, E. Vescovi, and A. Vezzani, Phys. Rev. A **85**, 043625 (2012).

[43] M. Kitagawa and M. Ueda, Phys. Rev. A **47**, 5138 (1993).

[44] D. J. Wineland, J. J. Bollinger, W. M. Itano, and D. J. Heinzen, Phys. Rev. A **50**, 67 (1994).

[45] V. S. Shchesnovich and M. Trippenbach, Phys. Rev. A **78**, 023611 (2008).

[46] B. Juliá-Díaz, T. Zibold, M. K. Oberthaler, M. Melé-Messeguer, J. Martorell, and A. Polls, Phys. Rev. A **86**, 023615 (2012).

[47] M. Gabbrielli, A. Smerzi, and L. Pezzè, Sci. Rep. **8**, 15663 (2018).